Applied Catalysis B: Environmental 160–161 (2014) 716–721

Contents lists available at ScienceDirect

Applied Catalysis B: Environmental

journal homepage: www.elsevier.com/locate/apcatb

# Effect of doping the nitrogen into carbon nanotubes on the activity of NiO catalysts for the oxidation removal of toluene

Shujuan Jiang[a], Eric Storr Handberg[a], Fen Liu[a], Yuting Liao[a], Huayu Wang[c,*], Zhe Li[b,*], Shaoqing Song[a,*]

[a] Key Laboratory of Radioactive Geology and Exploration Technology Fundamental Science for National Defense, School of Chemistry, Biology and Materials Science, East China Institute of Technology, Nanchang 330013, Jiangxi Province, PR China
[b] Key Laboratory of Catalysis and Materials Science of the State Ethnic Affairs Commission & Ministry of Education, South-Central University for Nationalities, Wuhan 430074, Hubei Province, PR China
[c] Jiangxi Institute of Measurement and Testing, Nanchang 330013, Jiangxi Province, PR China

ARTICLE INFO

*Article history:*
Received 25 March 2014
Received in revised form 8 June 2014
Accepted 17 June 2014
Available online 24 June 2014

*Keywords:*
Nitrogen doped carbon nanotube
NiO nanoparticles
The doped graphitic-like N
Oxidation removal of toluene

ABSTRACT

Nitrogen-doped carbon nanotubes (NCNTs) supported NiO (NiO/NCNTs) were prepared for catalyzing the oxidation removal of toluene. Characterization and catalysis tests showed the oxygen adspecies concentration and low-temperature reducibility of NiO/NCNTs increased with increasing the doped graphitic-like N ($N_G$) content of NCNTs, in good agreement with the trend of the catalytic performance of NiO/NCNTs. The optimized NiO/NCNTs-d catalyst with $N_G$ content of 6.22 at.% can achieve a completed conversion of toluene at 248 °C, and has a TOF value of nearly 10 times to NiO/CNTs at 160 °C. Therefore, these results may lead to a new strategy for exploring the advanced catalysts based on the carbon nanomaterials with abundant $N_G$ for the catalytic elimination of air pollutants.



## 1. Introduction

The catalytic oxidation removal of volatile organic compounds (VOCs, e.g., toluene) to control gaseous industrial emissions is considered as one of the most promising environmental technologies [1–3]. The key issue for such an approach is the availability of an effective catalyst. In the past years, the supported precious metal catalysts (e.g., Pt [4–14], Pd [15–24] and Au [25–30]) have been studied in the catalytic oxidation removal of VOCs. Although the supported Pt and Pd catalysts have shown the good catalytic activity at lower temperatures, their wide industrial applications are hindered by their high cost, low thermal stability, easy sintering and tendency to poisoning. As a potential alternative of precious metals, the supported transition metal oxides have received considerable attention in the oxidation removal of VOCs because they are low in cost and high in thermal stability [31–45]. Generally, catalytic performance of a transition metal oxide is mainly associated with the oxygen adspecies concentration and reducibility [30,31,43], which depends on the morphology, crystal size and exposed crystal face [31]. Interestingly, these physicochemical properties of transition metal oxides can also be facilely improved by the appropriate supports [44,45].

As a type of good candidate, carbonaceous materials have always attracted intense interest during the exploration of efficient catalysts from early activated carbon [46–50], to carbon nanofibers [9], carbon nanotubes for the catalytic oxidation of VOCs [45,51,52]. Recently, nitrogen doped CNTs (NCNTs) are considered as one of the promising supports due to the good electrical conductivity, mechanical strength as well as thermal stability [53]. Many studies have shown the benefits of using NCNTs as catalyst supports for Fischer–Tropsch [54], dehydrogenation [55] and fuel cell electrode reactions [56], resulting in an improved activity and/or production selectivity. The doped nitrogen in CNTs can mainly introduce two form species, i.e., pyridinic-like N ($N_P$) and graphitic-like N ($N_G$) [57]. The $N_P$ is a $sp^2$ hybridized nitrogen atom located at the openings or at defects of the graphitic sheets, while the $N_G$ is a carbon substituted nitrogen atom located within the graphitic matrix. The doping behavior with particular nitrogen can induce special electrical properties and chemical activities to CNTs [57]. However, few efforts have been made to investigate the effect of the doped nitrogen species of NCNTs on the physicochemical properties and

* Corresponding authors at: Key Laboratory of Radioactive Geology and Exploration Technology Fundamental Science for National Defense, East China Institute of Technology, School of Chemistry, Biology and Materials Science, Guanglan Road, Nanchang 330013, Jiangxi Province, China. Tel.: +86 791 83896550.
*E-mail address:* sqsong@ecit.edu.cn (S. Song).

http://dx.doi.org/10.1016/j.apcatb.2014.06.026
0926-3373/

activities of catalysts, although this may bring forth an unexpected catalytic performance due to the combination of the unique electronic and chemical properties. Thus, it will be very meaningful to investigate the effective nitrogen species of NCNTs for improving the activity of transition metal catalysts in the oxidation removal of VOCs. Herein, NiO nanoparticles (NPs) were supported on the surface of NCNTs. We studied which and further how the doped nitrogen species of NCNTs could influence physicochemical properties and catalytic activities of NiO/NCNTs in detail. Study results showed $N_G$ in NCNTs could promote NiO/NCNTs with high oxygen adspecies concentration and excellent reducibility, thus the so-constructed NiO/NCNTs presented high catalytic performance for the oxidation removal of toluene.

## 2. Experimental

### 2.1. Preparation of NCNTs and NiO/NCNTs

NCNTs were prepared by the chemical vapor deposition method with Fe–Co/γ-$Al_2O_3$ as catalyst and pyridine and/or 3-(aminomethyl)pyridine (AMP) as precursors.[57] The preparation process was as follows. Thirty milligram catalyst was placed in the reactor. After the reaction chamber was evacuated and flushed with $N_2$ for several times to remove oxygen and moisture, the reactor was heated to 750 °C. Three milliliter precursor was introduced into the furnace by an injection pump and carried to the reaction zone by argon flow of 1000 sccm for 15 min deposition. The nitrogen species and content were controlled by tuning the volume ratio of pyridine to AMP. The obtained NCNTs were denoted as NCNTs-a, NCNTs-b, NCNTs-c and NCNTs-d when the volume ratio of pyridine to 3-(aminomethyl)pyridine was 5, 3, 1 and 0, respectively. For comparison, CNTs were prepared by the similar method but with benzene as precursor. The as-prepared nanotubes were sequential refluxed in 6 M NaOH and 6 M HCl aqueous solution at 110 °C for 4 h, respectively. The purified NCNTs and CNTs were thoroughly washed with distilled water until the pH value of the filtrate reached 7, and then dried at 70 °C overnight. 0.5 g of the treated nanotubes were impregnated into 20 mL of $Ni(CH_3COO)_2$ aqueous solution under stirring followed by ultrasonic treatment for 25 min. Then the solvent was evaporated slowly under ambient conditions. The resulting solid mixture was gradually heated to 120 °C in air and kept for 3 h, then heated to 400 °C at a rate of 2 °C/min in He for 3 h. The sample was denoted as NiO/NCNTs-a, NiO/NCNTs-b, NiO/NCNTs-c, NiO/NCNTs-d or NiO/CNTs according to the obtained nanotubes. The loading amount of Ni for all catalysts was 15 wt.%.

### 2.2. Characterizations of the prepared samples

The metal catalyst residue in the purified NCNTs and Ni loading was analyzed by J-A1100 inductively coupled plasma (ICP, Jarrell-Ash, USA). X-ray diffraction (XRD) was performed on Philips X'pert Pro X-ray diffractometer with a Cu *K*α radiation at 40 kV. Transmission electron microscopy (TEM) measurements were carried out with JEOL-JEM-1010 transmission electron microscope at 100 kV. X-ray photoelectron spectroscopy (XPS) was carried out with an ESCALAB 250 electron spectrometer from Thermo of U.S.A. The C 1s peak signal at 284.6 eV was taken as a reference for the binding energy calibration. Temperature-programed reduction of hydrogen ($H_2$-TPR) was performed using a flow system equipped with a TCD detector. Typically, 50 mg of the samples was degassed at 100 °C for 1 h with argon gas flow, then cooled to 30 °C, and the gas flow was shifted to a mixture of 5 vol.% $H_2$ in Ar. The temperature was raised from 30 to 500 °C with a heating temperature rate of 10 °C/min. The water produced during reduction was trapped in a 5A molecular sieve column. Nitrogen sorption isotherms were measured at 77 K using Micromeritics equipment. The Brunauer–Emmett–Teller (BET) method and Barrett–Joyner–Halenda (BJH) models are used for specific surface area calculation and porosity evaluation, respectively.

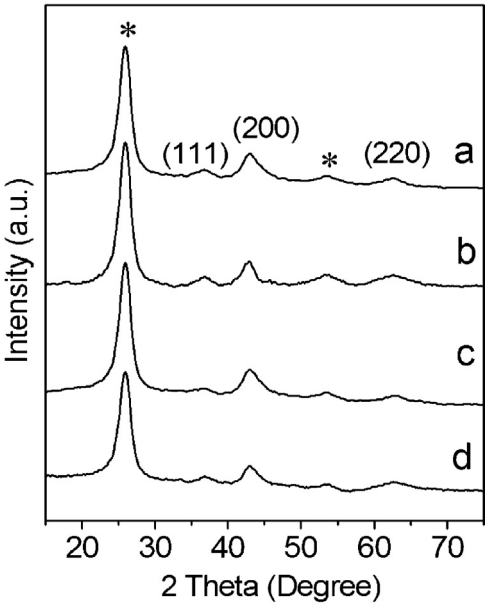


**Fig. 1.** XRD paterns for (a) NiO/NCNTs-a, (b) NiO/NCNTs-b, (c) NiO/NCNTs-c and (d) NiO/NCNTs-d.

### 2.3. Catalytic tests

The catalytic oxidation of toluene was performed in a quartz *U*-type tube microreactor under atmospheric pressure. In the catalytic process, 180 mg of catalyst was placed in the reactor and then suffered thermal treatment at 400 °C for 3 h. When the temperature of the reactor decreased to 100 °C, the reactant gas including 1000 ppm toluene, $O_2$ and $N_2$ (the molar ratio of toluene/$O_2$ is 1:400 and the space velocity (SV) is 20,000 mL/(g h)) was fed into the reactor with the flow rate of 60 mL/min. The reactants and products were analyzed by an online gas chromatograph with a thermal conductivity and a flame ionization detector. Porapak Q column was used to detect for $CO_2$ and hydrocarbons, and Molecular Sieve 5A for CO, $O_2$ and $N_2$. The outlet gases were also monitored online by a mass spectrometer (HPR20, Hiden). We found that no other products were detected in addition to $CO_2$ and $H_2O$.

## 3. Results and discussion

### 3.1. Crystal structure, morphology and surface area

The XRD pattern of each sample consists of five peaks which can be indexed to two composites (Fig. 1). The peaks at 26.1° and 54.2° (marked with *) are attributed to the (0 0 2) and (0 0 4) diffractions of graphite in the NCNTs (JCPDS 41-1487), while the ones at ~37.2°, 43.2° and 62.6° result from the (1 1 1), (2 0 0) and (2 2 0) diffractions of the cubic crystal structure of NiO (JCPDS 47-1049), indicating the formation of NiO species. The morphology of these NiO/NCNT catalysts was observed by TEM and the corresponding size distributions of overall particles. It can be seen that NCNTs with tubular structure have the diameters of around 20 nm (Fig. 2) and NiO NPs are homogeneously dispersed on the surface of NCNTs. Crystallite size distribution of NiO is around 3–10 nm with a similar average size of 5–7 nm for each NiO/NCNT catalyst (Fig. S1 in Supplementary materials. Surface areas of the NiO/NCNTs revealed by

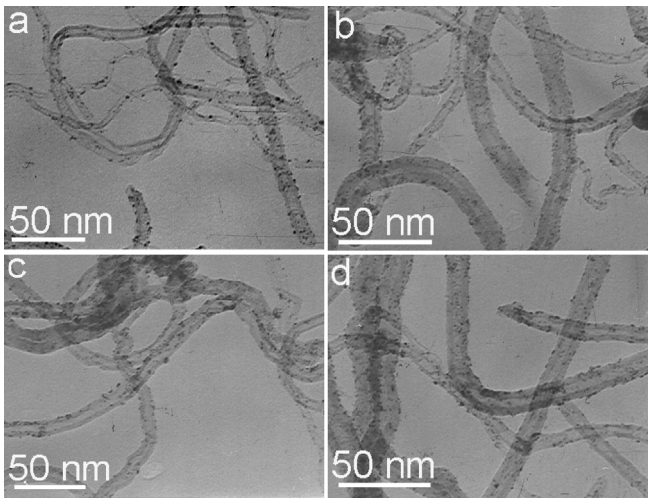


**Fig. 2.** TEM images of NiO/NCNT catalysts. (a) NiO/NCNTs-a, (b) NiO/NCNTs-b, (c) NiO/NCNTs-c and (d) NiO/NCNTs-d.

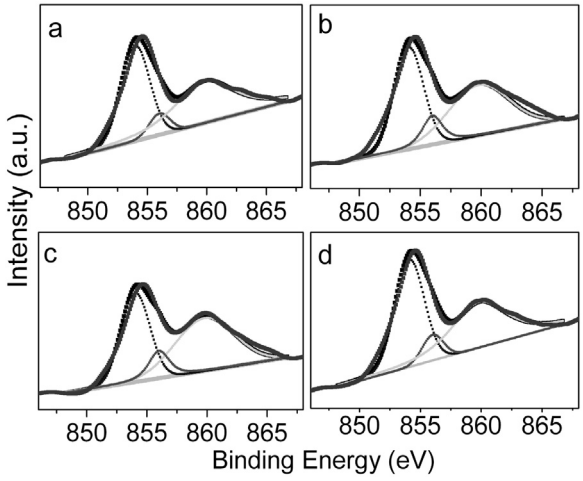


**Fig. 3.** Ni 2p XPS spectra. (a) NiO/NCNTs-a, (b) NiO/NCNTs-b, (c) NiO/NCNTs-c and (d) NiO/NCNTs-d.

BET method are similar to be 235.9, 237.5, 233.7 and 233.5 $m^2/g$ for the NiO/NCNTs-a, NiO/NCNTs-b, NiO/NCNTs-c and NiO/NCNTs-d, respectively.

### 3.2. Surface element composition and oxygen species

To guarantee an effective purification for NCNTs, XPS and ICP were used to detect the residue contents in the purified NCNTs (Fig. S2 and Table S1 in Supplementary materials). It is found that the NaOH/HCl treatment is an effective purification method. Then the element contents, chemical states and the surface adsorbed species of the NCNTs-based catalysts were investigated. Ni loading detected by ICP is 14.83, 14.85, 14.87 and 14.82% for NiO/NCNTs-a, NiO/NCNTs-b, NiO/NCNTs-c or NiO/NCNTs-d, respectively (Table 1). The XPS spectra of Ni 2p for the four samples covers the regions of 850–857.5 eV and 857.5–866 eV, corresponding to the Ni $2p_{3/2}$ and the satellite peak (Fig. 3). The Ni $2p_{3/2}$ signal of each catalyst can be deconvoluted into two components centered at 853.8 and 856.5 eV, ascribable to the characteristic of $Ni^{2+}$ and $Ni^{3+}$ species, respectively [31]. A quantitative analysis based on the integrated area of the two decomposed peaks could give rise to the relative proportion of the $Ni^{2+}$ to $Ni^{3+}$ species (Table 1). The molar ratio of $Ni^{2+}/Ni^{3+}$ is about 6/1 and showed no much change in all the prepared samples, suggesting the

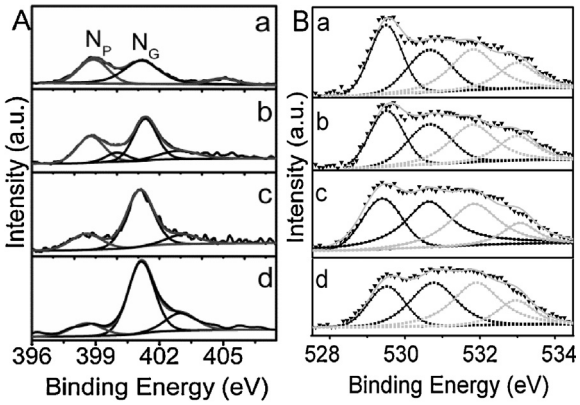


**Fig. 4.** (A) N 1s XPS spectra and (B) O 1s XPS spectra. (a) NiO/NCNTs-a, (b) NiO/NCNTs-b, (c) NiO/NCNTs-c and (d) NiO/NCNTs-d.

predominant existence of $Ni^{2+}$ and the consistent with the previous XRD result (Fig. 1). Meanwhile, the nitrogen species in NCNTs of NiO/NCNTs was revealed by N 1s XPS. Each N 1s spectrum is mainly comprised of $N_P$ and $N_G$ peaked at 399.1 and 401.3 eV (Fig. 4A) [57]. Interestingly, the intensity of peak increased at 401.3 eV while the opposite trend for the peak at 399.1 eV was witnessed with increasing the proportion of AMP in the precursors for the preparation. Simultaneously accompanied by the presentational changes of the two peaks, the content of $N_G$ increased progressively from 1.25 to 2.11, 4.05 and 6.22 at.% while that of $N_P$ decreased gradually from 1.08 to 0.95, 0.79 and 0.55 at.% in the corresponding NCNTs-a, NCNTs-b, NCNTs-c and NCNTs-d. These results indicate that a continuous modulation on the nitrogen species in NCNTs has been achieved, which provides a good platform for investigating the effective nitrogen in NCNTs of NiO/NCNTs for the catalytic oxidation of VOCs.

The surface oxygen species on the catalysts were analyzed by O 1s XPS (Fig. 4B). A broad and asymmetrical O 1s XPS peak for each sample was recorded, indicating the existence of several kinds of surface oxygen species. The oxygen species at BE of ~529.4, 530.4, 531.8 and 533.0 eV could be assigned to the surface lattice oxygen ($O_{latt}$), adsorbed oxygen ($O_{ads}$) species, hydroxyl and/or carbonate species, and adsorbed molecular water, respectively [30]. The quantitative result reveals that the molar ratio of $O_{ads}/O_{latt}$ for NiO/NCNTs-a, NiO/NCNTs-b, NiO/NCNTs-c and NiO/NCNTs-d gradually increases from 0.81 to 0.92, 1.43 and 1.56, respectively (Table 1). Compared with the pristine NiO NPs [58], NiO/NCNTs have a higher adsorbed oxygen concentration, which can be obviously mainly attributed to the NCNT support effect. Furthermore, combining with the XPS results of O 1s and N 1s spectra, we can definitely elucidate that the $N_G$ species in the supports plays a key role in the revolution of $O_{ads}/O_{latt}$ (Fig. S3 in Supplementary materials). Theoretical calculation shows carbon atoms adjacent to nitrogen in NCNTs possess a substantially high positive charge density to counterbalance the strong electronic affinity of the nitrogen atom [59]. Based on the principle of electroneutrality, $O_2$ can adsorb facilely on the NCNTs with a stable side-on chemisorption configuration, and subsequent O—O bond is stretched. Therefore, NCNTs as supports will favor to the enhancement of $O_{ads}/O_{latt}$ species on NiO/NCNTs.

### 3.3. $H_2$-TPR

The reduction behavior of NiO NPs dispersed on NCNTs was investigated by $H_2$-TPR since the redox behavior of the supported transition metal oxides was essential for the catalytic oxidation reaction. In Fig. 5, one main reduction step in the range of 200–400 °C can be clearly observed for each NiO/NCNT

**Table 1**
The chemical states and contents of Ni and N, as well as BET surface area of NiO/NCNTs.

| Catalysts | Surface composition | | | Ni loading (%) | BET surface area ($cm^2/g$) |
|---|---|---|---|---|---|
| | $Ni^{2+}/Ni^{3+}$ | $N_G/N_P$ | $O_{ads}/O_{latt}$ | | |
| NiO/NCNTs-a | 6.0 | 1.25/1.08 | 0.81 | 14.83 | 235.9 |
| NiO/NCNTs-b | 5.8 | 2.11/0.95 | 0.92 | 14.85 | 237.5 |
| NiO/NCNTs-c | 5.9 | 4.05/0.79 | 1.43 | 14.87 | 233.7 |
| NiO/NCNTs-d | 6.0 | 6.22/0.55 | 1.56 | 14.82 | 233.5 |

sample and the reduction temperature of NiO NPs is 268 °C (NiO/NCNTs-a), 248 °C (NiO/NCNTs-b), 237 °C (NiO/NCNTs-c) and 230 °C (NiO/NCNTs-d), respectively. Apparently, the reducibility of NiO/NCNTs has a strong dependence on the $N_G$ content of NCNTs, as reflected by a gradually lowering reduction temperature with increasing the $N_G$ constituent (Fig. S4 in Supplementary materials). Previous study considers that the $N_G$ atom can use three valence electrons for σ bonding with C and one for π bond, while the remaining one generates the π* state which activates the neighboring C atoms [60]. Thus, we deduced that the activated C atoms by $N_G$ on the surface of NCNTs could promote the activation and subsequent reduction of the supported NiO.

### 3.4. Catalytic performance

To guarantee the accuracy of the catalytic test, it is necessary to investigate the thermal stability of NiO/NCNTs, as determined by thermo gravimetric analysis in air (Fig. S5 in Supplementary materials). It is found the weight loss of the NiO/NCNT catalyst is negligible in all cases below 400 °C, which can ensure the catalytic stability during the catalytic oxidation of toluene operated below 400 °C.

The results of catalytic oxidation of toluene were recorded under the consecutively increasing temperature program, and the required reaction temperature was kept 20 min to ensure the accuracy of the data (Figs. S6–9 in Supplementary materials). The results of catalytic oxidation of toluene on the as-prepared catalysts presented that the toluene conversion increased normally with raising the reaction temperature in all cases (Fig. 6). It is noted that the catalytic reaction of toluene oxidation on NiO/CNTs starts at 120 °C and completes at 310 °C. Once introducing nitrogen to CNT support, the catalytic oxidation of toluene starts at 100 °C, and the completed reaction temperatures turn to be 290, 277, 268 and 248 °C for NiO/NCNTs-a, NiO/NCNTs-b, NiO/NCNTs-c and NiO/NCNTs-d catalyst, respectively, i.e., the catalytic performance follows the order: NiO/CNTs < NiO/NCNTs-a < NiO/NCNTs-b < NiO/NCNTs-c < NiO/NCNTs-d. As another kind of evaluation for catalytic activity, the turnover frequency (TOF) reflects the intrinsic catalytic capability of NiO NPs on different supports, which was calculated by using the conversion of toluene less than 10% based on the ~20% Ni dispersity (Fig. S10), and the results are listed in Table 2. It is seen that the NiO/NCNT catalysts show much higher TOF values than NiO/CNTs. For example, the TOF for the optimized NiO/NCNTs-d is $4.27 \times 10^{-5}$ ($s^{-1}$) at 160 °C, which is nearly 10 times to that for NiO/CNTs ($4.3 \times 10^{-6}$). This clearly indicates the distinct advantage of NCNTs as supports for the catalytic oxidation of toluene. Moreover, it can be seen that the catalytic activity sequence of NiO/NCNTs is consistent with the orders of oxygen adspecies concentration obtained in the XPS studies and low-temperature reducibility revealed by the $H_2$-TPR investigations. Thus, the enhancement of catalytic performance over NiO/NCNTs is essentially attributed to the effect of $N_G$ doped in NCNTs.

### 3.5. The kinetics of the catalytic oxidation

In the catalytic oxidation reaction of VOC, the reaction rate based on the kinetic model can be expressed as the following equation [9]:

$$-r_i = \frac{dC_i}{dt} = kC_i^n C_{O_2}^m \quad (1)$$

$C_{O_2}$ and $C_i$ correspond to the concentration of $O_2$ and toluene, $k$ the reaction rate, and $m$, $n$ the reaction order. Here, $C_{O_2}$ is much higher than $C_i$ (the molar ratio of toluene/$O_2$ is 1:400), and thus $C_{O_2}$ can be considered as constant during the reaction. Eq. (1) can be simplified as the following equation:

$$-r_i = \frac{dC_i}{dt} = KC_i^n \quad (2)$$

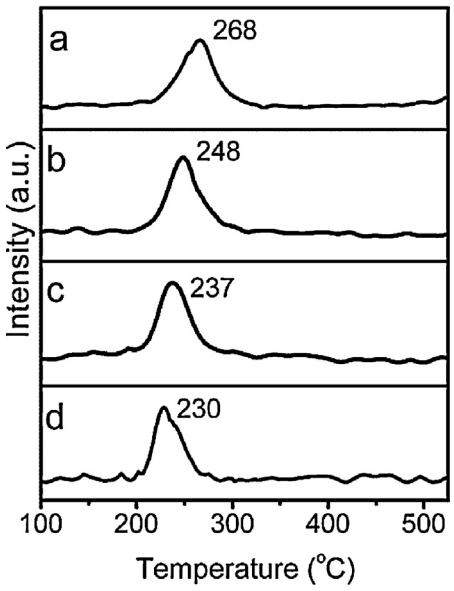


**Fig. 5.** $H_2$-TPR spectra for (a) NiO/NCNTs-a, (b) NiO/NCNTs-b, (c) NiO/NCNTs-c and (d) NiO/NCNTs-d.

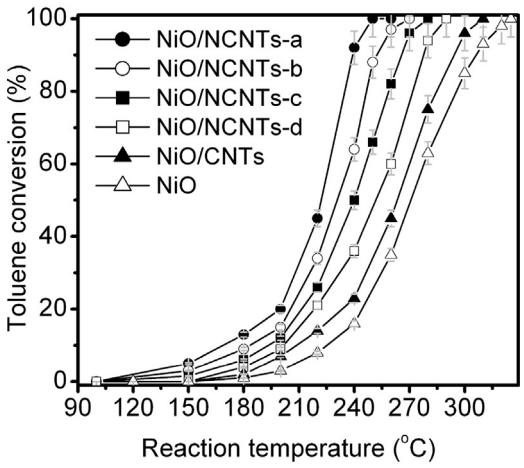


**Fig. 6.** the toluene conversion vs. reaction temperature catalyzed by NiO/NCNTs-a, NiO/NCNTs-b, NiO/NCNTs-c, NiO/NCNTs-d and NiO/CNTs.

**Table 2**
TOF data for the catalysts at different temperatures. The TOF data were determined under 22 the conditions of $C_i$ = 1000 ppm, conversion of toluene <10%, molar ratio of toluene/$O_2$ = 1/400, SV = 20,000 mL/(g h) at the temperature of 160, 165 or 170 °C.

| Temperature (°C) | NiO/NCNTs-d | NiO/NCNTs-c | NiO/NCNTs-b | NiO/NCNTs-a | NiO/CNTs |
|---|---|---|---|---|---|
| 170 | $5.53 \times 10^{-5}$ | $3.86 \times 10^{-5}$ | $2.32 \times 10^{-5}$ | $1.53 \times 10^{-5}$ | $7.3 \times 10^{-6}$ |
| 165 | $5.01 \times 10^{-5}$ | $3.33 \times 10^{-5}$ | $2.04 \times 10^{-5}$ | $1.27 \times 10^{-5}$ | $7.1 \times 10^{-6}$ |
| 160 | $4.27 \times 10^{-5}$ | $2.28 \times 10^{-5}$ | $1.48 \times 10^{-5}$ | $9.6 \times 10^{-6}$ | $4.3 \times 10^{-6}$ |

$K$ is the apparent reaction rate ($K = kC_{O_2}^m$). Therefore, the linear relationship of $\ln(-r_i)$ and $\ln C_i$, and $n$ as well as $\ln K$ can be obtained by altering $C_i$ (Table S3 in SI). It is seen that the oxidation of toluene obeys a 0.29 and 0.35-order reaction mechanism on NiO/NCNTs and NiO/CNTs, respectively. According to Arrhenius equation (Eq. (3)):

$$K = -A\exp\left(\frac{-E_a}{RT}\right) \quad (3)$$

$A$ is the pre-exponential factor, $E_a$ the apparent activation energy (kJ/mol) and $T$ the reaction temperature. Arrhenius plots reflect the correlation of the variation of $K$ values with $T$, and the plots here are derived within 10% of the toluene conversion. The values of $K$, $A$ and $E_a$ of toluene oxidation over the catalysts can be subsequently obtained based on the slopes of the Arrhenius plots. It is seen the $K$ value increases with increasing the reaction temperature for each catalyst (Fig. 7). Meanwhile, at the same temperature, the $K$ values for all NiO/NCNT catalysts are much higher than that for the NiO/CNT catalyst, and follow the order: NiO/NCNTs-a < NiO/NCNTs-b < NiO/NCNTs-c < NiO/NCNTs-d. Furthermore, the $E_a$ values of the NiO/NCNTs catalysts (58–76 kJ/mol) are greatly reduced compared with that of NiO/CNT catalyst. In detail, $E_a$ is in the sequence of NiO/NCNTs-d (58 kJ/mol) < NiO/NCNTs-c (60 kJ/mol) < NiO/NCNTs-b (63 kJ/mol) < NiO/NCNTs-a (76 kJ/mol) < NiO/CNTs (78 kJ/mol). The results indicate that the lower the $E_a$ value is, the easier will the complete oxidation of organics proceed, indicating the better performance of the catalyst.

### 3.6. Catalytic stability

The 25 h on-stream toluene oxidation experiment over the NiO/NCNTs-d was carried out at 240 °C with a ~90% conversion of toluene (Fig. 8A). No significant loss in catalytic activity was detected in the direct test at 240 °C. After increasing the reaction temperature up to 350 °C or 400 °C, the catalyst still could present a good stability. However, the conversion of toluene on NiO/NCNTs-d decreases to 83% or 76% after further enhancing the reaction temperature to 450 or 480 °C, which is mainly attributed to the destroyed structure of NCNTs after a heating treatment.

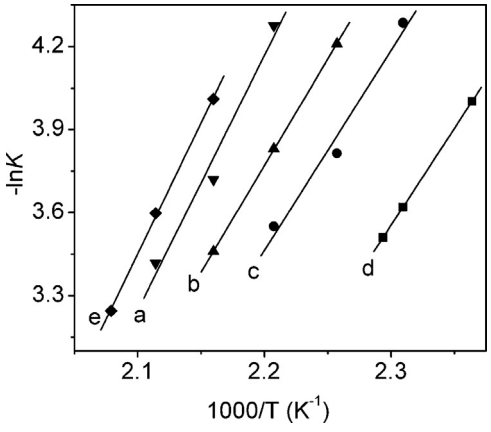


**Fig. 7.** Arrhenius plots for the catalytic oxidation of toluene over NiO/NCNTs-a (a), NiO/NCNTs-b (b), NiO/NCNTs-c (c), NiO/NCNTs-d (d), and NiO/CNTs (e).

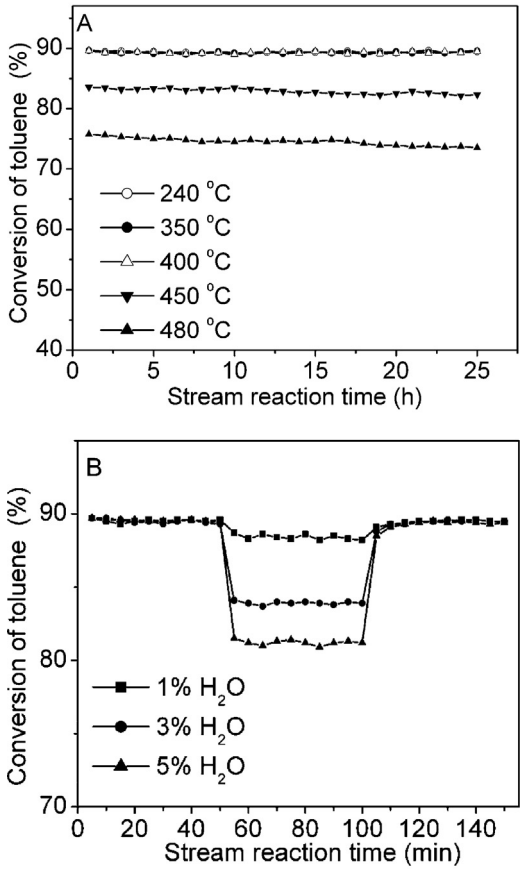


**Fig. 8.** (A) Time-on-stream behaviors of the catalytic oxidation for toluene on NiO/NCNTs-d catalyst at 240, 350, 400, 450 and 480 °C. (B) Effect of water vapor on the catalytic activity of the NiO/NCNTs-d under the same reaction conditions.

Moreover, the effect of water vapor (1.0, 3.0, or 5.0 vol.%) on the catalytic performance of NiO/NCNTs was investigated at 240 °C with SV = 20,000 mL/(g h) (Fig. 8B). After introducing a 1.0 vol.% water vapor to the reaction system, only about 2% loss was observed in toluene conversion. When 3.0 or 5.0 vol.% water vapor was introduced, the toluene conversion decreased to 83% and 81%. This inhibition effect of water vapor can be attributed to the competitive adsorption of water and toluene as well as oxygen molecules [61]. Interestingly, toluene conversions could be restored without water vapor input.

## 4. Conclusion

NCNTs with graphitic nitrogen as supports could greatly enhance the catalytic performance of NiO for the catalytic oxidation of toluene, as reflected by the lowered apparent activation energy and the completed conversion temperature of toluene oxidation along with increasing the graphitic nitrogen content of NCNTs in NiO/NCNTs. The high catalytic activity of NiO/NCNTs could be attributed to (i) the good low-temperature reducibility of NiO/NCNTs and (ii) the high concentration of adsorbed oxygen

species. These results strongly suggest that enhancing the activities of transition metal oxides by using carbon-based support materials doped with graphitic nitrogen is a practical strategy for designing highly efficient catalysts for the removal of VOCs.

## Acknowledgments

We gratefully acknowledge the support from the National Natural Science Foundation of China (21103019, 21307011 and 21303271), the Foundation of Key Laboratory of Radioactive Geology and Exploration Technology Fundamental Science for National Defense (RGET1214 and RGET1312) and the Start-up Fund of the East China Institute of Technology (DHBK1005 and DHBK1009).

## Appendix A. Supplementary data

Supplementary data associated with this article can be found, in the online version, at http://dx.doi.org/10.1016/j.apcatb.2014.06.026.

## References

[1] K. Everaert, J. Baeyens, J. Hazard. Mater. 109 (2004) 113–139.
[2] Y.S. Xia, H.X. Dai, H.Y. Jiang, J.G. Deng, H. He, C.T. Au, Environ. Sci. Technol. 43 (2009) 8355–8360.
[3] P. Papaefthimiou, T. Ioannides, X.E. Verykios, Appl. Catal., B: Environ. 13 (1997) 175–184.
[4] P. Papaefthimiou, T. Ioannides, X.E. Verykios, Appl. Catal., B: Environ. 15 (1998) 75–92.
[5] M.P. Pina, S. Irusta, M. Menendez, J. Santamaria, R. Hughes, N. Boag, Ind. Eng. Chem. Res. 36 (1997) 4557–4566.
[6] J. Corella, J.M. Toledo, A.M. Padilla, Appl. Catal., B: Environ. 27 (2000) 243–256.
[7] A. Koyer-Golkowska, A. Musialik-Piotrowska, J.D. Rutkowski, Catal. Today 90 (2004) 133–138.
[8] K. Bendahou, L. Cherif, S. Siffert, H.L. Tidahy, H. Benaissa, A. Aboukais, Appl. Catal., A: Gen. 351 (2008) 82–87.
[9] S. Morales-Torres, A.F. Perez-Cadenas, F. Kapteijn, F. Carrasco-Marin, F.J. Maldonado-Hodar, J.A. Moulijn, Appl. Catal., B: Environ. 89 (2009) 411–419.
[10] T.F. Garetto, C.R. Apesteguia, Catal. Today 62 (2000) 189–199.
[11] K.J. Kim, H.G. Ahn, Appl. Catal., B: Environ. 91 (2009) 308–318.
[12] A.C. Gluhoi, N. Bogdanchikova, B.E. Nieuwenhuys, Catal. Today 113 (2006) 178–181.
[13] Q.H. Xia, K. Hidajat, S. Kawi, Catal. Today 68 (2001) 255–262.
[14] H.S. Kim, T.W. Kim, H.L. Koh, S.H. Lee, B.R. Min, Appl. Catal., A: Gen. 280 (2005) 125–131.
[15] C. He, J.J. Li, P. Li, J. Cheng, Z.P. Hao, Z.P. Xu, Appl. Catal., B: Environ. 96 (2010) 466–475.
[16] J.J. Li, Z. Jiang, Z.P. Hao, X.Y. Xu, Y.H. Zhuang, J. Mol. Catal. A: Chem. 225 (2005) 173–179.
[17] S.C. Kim, W.G. Shim, Appl. Catal., B: Environ. 92 (2009) 429–436.
[18] S.C. Kim, S.W. Nahm, W.G. Shim, J.W. Lee, H. Moon, J. Hazard. Mater. 141 (2007) 305–314.
[19] L.F. Liotta, Appl. Catal., B: Environ. 100 (2010) 403–412.
[20] C. He, P. Li, H.L. Wang, J. Cheng, X.Y. Zhang, Y.F. Wang, Z.P. Hao, J. Hazard. Mater. 181 (2010) 996–1003.
[21] C. He, J.J. Li, j. Cheng, L.D. Li, P. Li, Z.P. Hao, Z.P. Xu, Ind. Eng. Chem. Res. 48 (2009) 6930–6936.
[22] J.J. Li, X.Y. Xu, Z. Jiang, Z.P. Hao, C. Hu, Environ. Sci. Technol. 39 (2005) 1319–1323.
[23] C. He, L.L. Xu, L. Yue, Y.T. Chen, J.S. Chen, Z.P. Hao, Ind. Eng. Chem. Res. 51 (2012) 7211–7222.
[24] L.Y. Jin, R.H. Ma, J.J. Lin, L. Meng, Y.J. Wang, M.F. Luo, Ind. Eng. Chem. Res. 50 (2011) 10878–10882.
[25] S. Scire, S. Minico, C. Crisafulli, C. Satriano, A. Pistone, Appl. Catal., B: Environ. 40 (2003) 43–49.
[26] C.Y. Ma, D.H. Wang, W.J. Xue, B.J. Dou, H.L. Wang, Z.P. Hao, Environ. Sci. Technol. 45 (2011) 3628–3634.
[27] J.J. Li, C.Y. Ma, X.Y. Xu, J.J. Yu, Z.P. Hao, S.Z. Qiao, Environ. Sci. Technol. 42 (2008) 8947–8951.
[28] B.B. Chen, X.B. Zhu, M. Crocker, Y. Wang, C. Shi, Appl. Catal., B: Environ. 154–155 (2014) 73–81.
[29] B.B. Chen, C. Shi, M. Crocker, Y. Wang, A.M. Zhu, Appl. Catal., B: Environ. 132–133 (2013) 245–255.
[30] Y.X. Liu, H.X. Dai, J.G. Deng, S.H. Xie, H.G. Yang, W. Tan, W. Han, Y. Jiang, G.S. Guo, J. Catal. 309 (2014) 408–418.
[31] G.M. Bai, H.X. Dai, J.G. Deng, Y.X. Liu, W.G. Qiu, Z.X. Zhao, X.W. Li, H.G. Yang, Chem. Eng. J. 219 (2013) 200–208.
[32] X.D. Ma, X. Feng, J. Guo, H.Q. Cao, X.Y. Suo, H.W. Sun, M.H. Zheng, Appl. Catal., B: Environ. 147 (2014) 666–676.
[33] B.D. Rivas, C. Sampedro, M. García-Real, R. López-Fonseca, J.I. Gutiérrez-Ortiz, Appl. Catal., B: Environ. 129 (2013) 225–235.
[34] C.H. Zhang, Y.L. Guo, Y. Guo, G.Z. Lu, A. Boreave, L. Retailleau, A. Baylet, A. Giroir-Fendler, Appl. Catal., B: Environ. 148–149 (2014) 490–498.
[35] L. Zeng, W.L. Song, M.H. Li, D.W. Zeng, C.S. Xie, Appl. Catal., B: Environ. 147 (2014) 490–498.
[36] Z. Wang, G.L. Shen, J.Q. Li, H.D. Liu, Q. Wang, Y.F. Chen, Appl. Catal., B: Environ. 138–139 (2013) 253–259.
[37] C. He, Y.K. Yu, L. Yue, N.L. Qiao, J.J. Li, Q. Shen, W.J. Yu, J.S. Chen, Z.P. Hao, Appl. Catal., B: Environ. 147 (2014) 156–166.
[38] L.Y. Lin, H.L. Bai, Appl. Catal., B: Environ. 148–149 (2014) 366–376.
[39] C. Gannoun, A. Turki, H. Kochkar, R. Delaigle, P. Eloy, A. Ghorbel, E.M. Gaigneaux, Appl. Catal., B: Environ. 147 (2014) 58–64.
[40] B.Y. Bai, H. Arandiyan, J.H. Li, Appl. Catal., B: Environ. 142–143 (2013) 677–683.
[41] B.D. Rivas, R. Lopez-Fonseca, C. Jomenez-Gonzalez, J.I. Gutierrez-Ortiz, Chem. Eng. J. 184 (2012) 184–192.
[42] B.D. Rivas, R. Lopez-Fonseca, C. Jomenez-Gonzalez, J.I. Gutierrez-Ortiz, J. Catal. 281 (2011) 88–97.
[43] F. Wang, H.X. Dai, J.G. Deng, G.M. Bai, K.M. Ji, Y.X. Liu, Environ. Sci. Technol. 46 (2011) 4034–4041.
[44] G.S. Pozan, J. Hazard. Mater. 221–222 (2012) 124–130.
[45] S.J. Jiang, S.Q. Song, Appl. Catal., B: Environ. 140–141 (2013) 1–8.
[46] M.A. Alvarez-Merino, M.F. Ribeiro, J.M. Silva, F. Carrasco-Marin, F.J. Maldonado-Hodar, Environ. Sci. Technol. 38 (2004) 4664–4670.
[47] J. Bedia, J.M. Rosas, J. Rodriguez-Mirasol, T. Cordero, Appl. Catal., B: Environ. 94 (2010) 8–18.
[48] C.Y. Lu, M.Y. Wey, Fuel Process. Technol. 88 (2007) 557–567.
[49] C.Y. Lu, M.Y. Wey, L.L. Chen, Appl. Catal., A: Gen. 325 (2007) 163–174.
[50] S. Morales-Torres, F.J. Maldonado-Hódar, A.F. Pérez-Cadenas, F. Carrasco-Marín, J. Hazard. Mater. 183 (2010) 814–822.
[51] K.H. Chuang, Z.S. Liu, C.Y. Lu, M.Y. Wey, Ind. Eng. Chem. Res. 48 (2009) 4202–4209.
[52] A.M. Nie, H.S. Yang, Q. Li, X.Y. Fan, F.M. Qiu, X.B. Zhang, Ind. Eng. Chem. Res. 50 (2011) 9944–9948.
[53] S.J. Jiang, Y.W. Ma, G.Q. Jian, H.S. Tao, X.Z. Wang, Y.N. Fan, Y.N. Lu, Z. Hu, Y. Chen, Adv. Mater. 21 (2009) 4953–4956.
[54] J.Z. Lu, L.J. Yang, B.L. Xu, Q. Wu, D. Zhang, S.J. Yuan, Y. Zhai, X.Z. Wang, Y.N. Fan, Z. Hu, ACS Catal. 4 (2014) 613–621.
[55] L.M. Ombaka, P. Ndungu, V.O. Nyamori, Catal. Today 217 (2013) 65–75.
[56] B.P. Vinayan, S. Ramaprabhu, Nanoscale 5 (2013) 5109–5118.
[57] H. Chen, Y. Yang, Z. Hu, K.F. Hu, Y.W. Ma, Y. Chen, X.S. Wang, Y.N. Lu, J. Phys. Chem. B 110 (2006) 16422–16427.
[58] G.M. Bai, H.X. Dai, J.G. Deng, Y.X. Liu, K.M. Ji, Catal. Commun. 27 (2012) 148–153.
[59] X.B. Hu, Y.T. Wu, H.R. Li, Z.B. Zhang, J. Phys. Chem. C 114 (2010) 9603–9607.
[60] K.P. Gong, F. Du, Z.H. Xia, M. Durstock, L.M. Dai, Science 323 (2009) 760–764.
[61] W. Han, J.G. Deng, S.H. Xie, H.G. Yang, H.X. Dai, C.T. Au, Ind. Eng. Chem. Res. 53 (2014) 3486–3494.